

Effect of laser additive manufacturing parameters on hardness and geometry of Inconel 625 parts manufactured by direct laser metal deposition

Mobin Nankali¹, Javad Akbari¹, Mahmoud Moradi^{2*}, Zeinab Malekshahi Beiranvand³

1- Department of Mechanical Engineering, Sharif University of Technology, Tehran, Iran

2- School of Mechanical, Aerospace and Automotive Engineering, Faculty of Engineering, Environment and Computing, Coventry University, Gulson Road, Coventry, CV1 2JH, United Kingdom.

3- Department of Materials science and Engineering, Tarbiat Modares University, Tehran, Iran.

Abstract

This research investigates the effect of process parameters on the geometry and properties of In625 parts, manufactured by the direct laser metal deposition (DLMD) process. For this purpose, eight parts, consisting of 5 layers on top of each other, were manufactured, and the effect of laser power, laser focal plane position, and scanning speed on the height, width, and surface smoothness of each of them was investigated using design of experiment (DOE). The experimental results showed that the height of the parts manufactured by 800 W/mm and 200 W/mm of energy density is 3.69 mm and 6.12 mm, respectively. The thickness of the parts manufactured by 80 W/mm and 200 W/mm of energy density is 1.5 mm and 3.47 mm, respectively, and the mass of powders deposited at the scanning speed of 2.5 mm/s and 1.5 mm/s is 3.4 gr and 5.66 gr, respectively. Also, the combination of experimental and DOE data showed that the effect of laser power and scanning speed on the thickness of the parts is more significant than the effect of laser focal plane position and is inversely related to scanning speed, and directly related to the laser power. Also, the effect of scanning speed and laser focal plane position on the height of the parts is more significant than the effect of laser power. It is also shown that the effect of laser power and laser focal plane position on the surface smoothness is more significant than other parameters.

Keywords: additive manufacturing, metal 3D printing, direct laser metal deposition, geometry dimension.

1. Introduction

Nowadays, additive manufacturing (AM) is one of the new methods of rapid prototyping. AM provides the ability to fabricate new geometries, materials with excellent properties and variable composition, as well as material recycling [1]. One of the most common methods of AM is DLMD, also known as laser powder forming (LPF). In this process, the powder is sprayed by the nozzle to the target area on the substrate and melts the powder using a laser beam that is applied to the target area, and forms a melt pool, resulting in a layer of material is formed. By repeating this process, the following layers are formed on the substrate. Fig. 1 shows a schematic of this process.

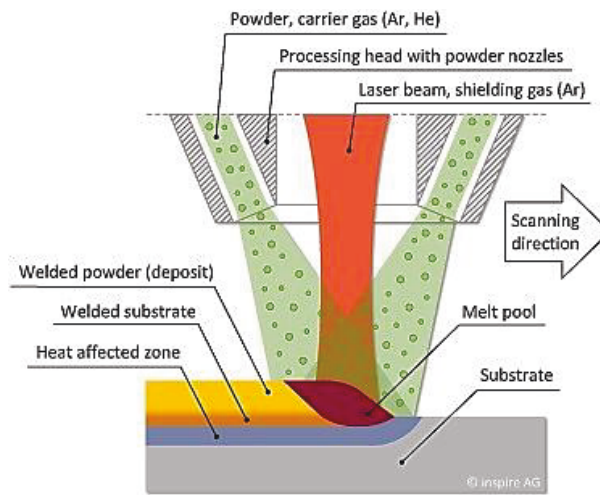


Figure 1 - Schematic of the DMD process [2].

Extensive research has been done in the field of powder additive manufacturing on a wide range of materials such as nickel, iron, cobalt, and titanium alloys, as well as metallic, and ceramic composites in which researchers studied the mechanical and microstructural properties, intending to increase the quality and dimensional accuracy of the parts manufactured by this method. Debroy et al. [3] showed that the parameters of additive manufacturing, including laser beam power, scanning speed, and fabrication direction in the DMD process, have a significant influence on the strength of manufactured parts. In another study, Rio et al. [4] examined the effect of energy density on the tensile strength of Inconel 625 and 316 steel parts produced by LMD, and they showed that the tensile strength decreases with increasing energy density. Taberner et al. [5] showed the effect of DLMD process parameters on the mechanical properties of Inconel 718 specimens. In another study, direct laser metal deposition (DLMD) experiments for Inconel 718 Superalloy were conducted to examine the effects of scanning speed as well as

powder feed rate on the process [6]. Polo et al. [7] also showed that by optimizing the manufacturing parameters, the manufacturing time could be reduced, and the tensile strength can be improved. Mesomedier et al. [7] showed that increasing the laser focal plane position increases the dimensions of the molten pool and the surface smoothness. Moktofogima et al. [8] showed that with increasing laser power, the depth and the thickness of the molten pool and porosity increase. Moradi et al. [9] showed that the laser power reduction is effective on the hardness of Stalite 6 laser manufactured parts, and with employing a strategy of power reduction from the first layer to upward in comparison to constant laser power strategy; the Hardness became lower and more significant, respectively. They also showed that [10] increasing the laser power has a reverse impact on the height and stability of the parts manufactured by DLMD. The other result of this study was that varying the focal plane position of the laser beam in the powder stream has a significant effect on the manufactured part quality. Nickel-based superalloys are used for high-performance components in jet engines and gas turbines due to their creep resistance, tensile properties, and corrosion/oxidation resistance. Due to the very high strength of many nickel-based superalloys such as Inconel 625, machining and forming them are expensive. Therefore, the DMD process can be an excellent alternative method for the fabrication of these parts.

So far, no comprehensive study has been presented that shows the effect of all main process parameters of direct laser metal deposition and their optimization via statistical methods on the properties and quality of manufactured parts. In this study, the effect of process parameters, including laser power, scanning speed, and laser focal plane position, on the properties of Inconel 625 parts made by the DMD method has been investigated. Furthermore, the effect of these three parameters on the Hardness and dimensional parameters of the parts has been examined, using DOE to create the maximum surface smoothness.

2. Experimental methods

In this study, for the DLMD process, a continuous fiber laser source with a maximum power of 1000 watts, and four nozzles were used to spray the powder. A three-axis CNC table was used. According to earlier research [9, 10], the most suitable range for laser power between 200 to 300 watts was selected. According to the earlier tests performed with the device on various powders, the best setup for the powder sprayer occurs when the mixer of the powder sprayer is

set to 30%. So, the powder flow rate was considered constant, and the effect of three parameters of laser power, laser focal plane position, and scanning speed was investigated. To prevent the change of powder spraying method, the distance of the substrate to the surface of the part of the earlier pass was considered constant, and only the laser focal plane position was changed with an adjusting screw between -4 to +4 mm. In these experiments, the layering was in a one-way direction. After each layering, it was given 30 seconds, until the temperature was uniform throughout the part, and then the next layer was generated. Argon gas has also been used to prevent rapid oxidation of the molten pool, and a gas flow rate of 3 l/min was considered. The carrier gas is dry argon, which first enters the powder flow device, and after mixing with the metal powder, moves to the nozzles. The carrier gas flow rate was considered to be 1.5 l / min. The powder used in this process was Inconel 625 made by the gas pressure atomizing method. Fig. 2 shows the dimensional distribution and geometric shape of the powder particles. It should be noted that the surface smoothness and the sphericity of the powder are critical to the flow of powder easily in the nozzles.

The chemical composition of the powder and substrate is shown in Table 1. The substrate material used in the experiment is hot work tool steel 2344 with dimensions of $1 \times 7 \times 10 \text{ cm}^3$.

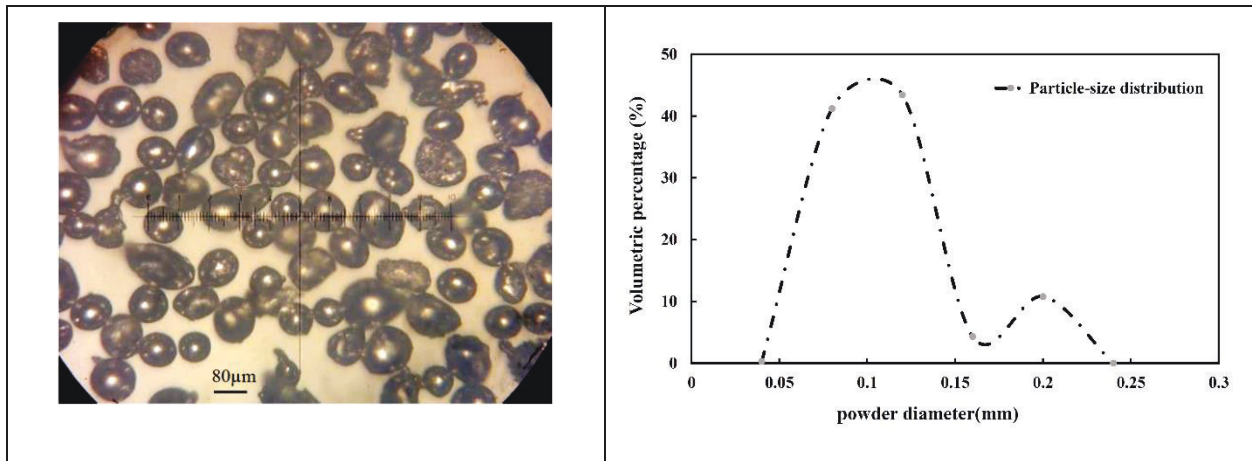


Figure 2 - Morphology and dimensional distribution of the powder used in the experiment

S	P	V	Mn	O	C	Si	Fe	Nb	Mo	Cr	Ni	
----------	----------	----------	-----------	----------	----------	-----------	-----------	-----------	-----------	-----------	-----------	--

-	-	-	0.33	0.24	0.02	1.05	1.39	2.67	9.06	21.22	Balance	Powder (Inconel 625)
0.015	0.024	1.01	0.37	-	0.36	0.99	91.14	-	1.05	5.03	-	Substrate (steel 2344)

Table 1- Chemical composition of powder and substrate

2.1.Full factorial design

Design of experiments (DOE) involves a series of experiments that deliberately modify the input variables of the process, and then detect the variation in the output response of the process [7-9]. Full factorial design is a mathematical and statistical method that is valuable for analyzing and modeling issues affected by several variables and aims to optimize the response [11, 12]. In most issues related to full factorial design, the relationship between the output response and the independent variables is unknown. For this reason, the first step in full factorial design Methodology is to find approximations for the actual relationship between the responses and the set of independent variables. Usually, low-order polynomials are used with independent variables. If there is any curvature in the system, then higher-order polynomials need to be used. Equation 1 presents the general form of the polynomial Equation [13];

$$y = \beta_0 + \sum_{i=1}^k \beta_i x_i + \sum_{i=1}^k \beta_{ii} x_i^2 + \sum_i \sum_j \beta_{ij} x_i x_j + \varepsilon \quad (1)$$

In this Equation, β is a constant parameter, β_i is a linear coefficient, β_{ii} is a quadratic coefficient, β_{ij} is an interaction coefficient, and ε is the error of the parameters of the regression. In almost all responses, one or some of these approximation polynomials are used [14].

In this research, the scanning speed, laser power, and the laser focal plane position were considered independent input variables. Three input parameters of the experiment, giving coded values, and actual values depicted in Table 3.

The number of tests will be calculated from Equation 2:

(2)	$DOE = 2^n = 2^3 = 8$
------------	-----------------------

Where n is the number of parameters. Therefore, the number of tests that must be performed for the three parameters is at least 8. To further investigate the laser focal plane position, two more experiments were added to the experiments. In Table 2, there are two upper and lower limits for each parameter.

Table 2 - Range of parameters

Parameter	-1	+1
Power laser (W)	200	300
Focal plane position (mm)	Large (-2)	Small (+2)
Scanning speed (mm/s)	1.5	2.5

As shown in Fig. 3 in mode -2, the laser spot point is located 2 mm above the powder concentration plane, while in +2 mode, and it is located 4 mm lower down the powder concentration plane.

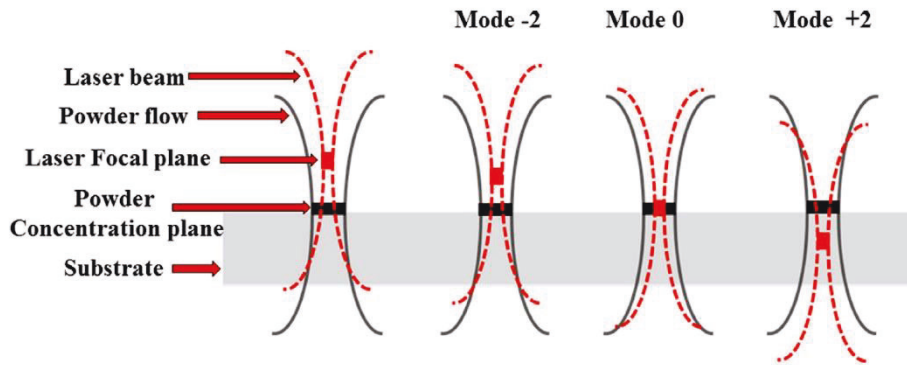


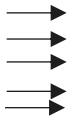
Figure 3- Variation of the laser focal plane position in the powder stream [11].

Table 3 shows the experimental combination by the full fractional design method. The value -1 shows the lower limit and +1 the upper limit of the parameter. Table 4 shows the constant values of the process.

Table 3 - Used parameters for test combination

Main variables			Coded variables			Test number	Part number
Focal plane position (mm)	Laser power (W)	Scanning speed (mm/s)	Focal plane position (mm)	Laser power (W)	Scanning speed (mm/s)		
Large(-2)	300	2.5	-1	+1	+1	1	1
Large(-2)	200	2.5	-1	-1	+1	2	2
Small(+2)	200	2.5	+1	-1	+1	3	3
Small(+2)	200	1.5	+1	-1	-1	4	4
Small(+2)	300	2.5	+1	+1	+1	5	5
Small(+2)	300	1.5	+1	+1	-1	6	6
Large(-2)	300	1.5	-1	+1	-1	7	7
Large(-2)	200	1.5	-1	-1	-1	8	8

Table 4- Process constant values of DLMD

Head distance from the part surface (mm)	Flow rate of powder carrier gas (l / min)	Flow rate of axial gas (l / min)	Flow rate of powder	Advance forward perpendicular to the table	Number of layers	Scan method	Delay time (s)
15	1.5	3	30%	0.6	5		30s

After fabrication of the parts, first, surface smoothness, average height, and profile of a cross-section of the parts were measured using Vision Measuring Machine (VMM) device. In this device, the parts are placed under the camera, and points are placed on it, and dimensions are extracted based on the points on the figure. Fig. 4 shows how to measure the average surface smoothness with this device.

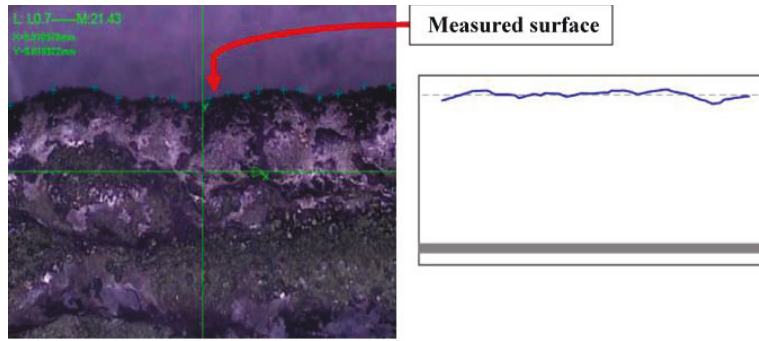


Figure 4- Measurement of surface smoothness using VNM device.

The average level of smoothness is calculated from Equation 3. The average thickness and height of the parts were measured similarly.

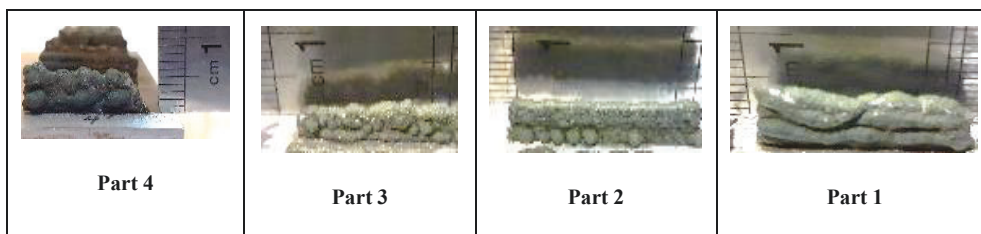
(3)	$R_a = \frac{1}{N} \sum_{i=1}^N fn $
------------	---------------------------------------

By dimensional measurements, the specimens were mounted for Vickers Hardness tests.

3. Results and discussion

The purpose of the experiments was to investigate the effect of three parameters of laser power, laser focal plane position, and scanning speed, and thus to investigate the effect of energy density on the quality of the parts, including geometry and hardness of the parts. Based on the parameters of the test combination in Table 3, 10 parts were manufactured. Fig. 5 shows the parts made using these parameters.

As can be seen, the process parameters are very effective on the quality of the parts. Fig. 6 also shows images of the wall and surface of part No. 9 as a part with optimal parameters. Table 5 shows the results of dimensional and Hardness measurements for each part.



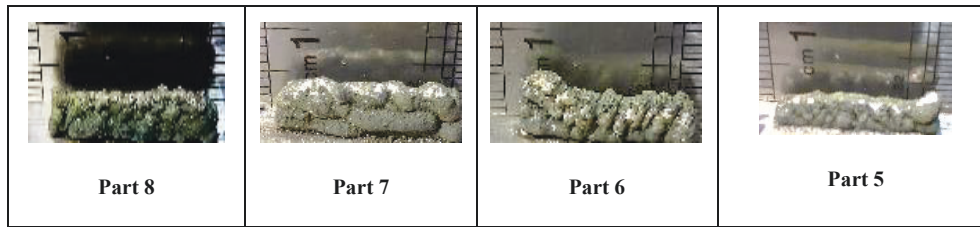


Figure 5- Experimental parts

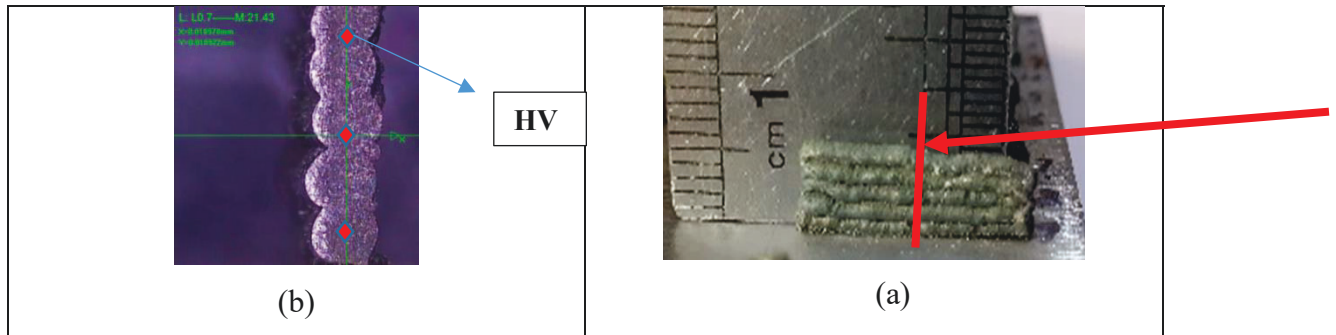


Figure 6- Parts (9) with optimal parameters a) Overview of the manufactured part, b) Cross-section of the part

Table 5 - Results of dimensional and Hardness measurements for each part

Input parameters				Output data			
Test number	Scanning speed (mm/s)	Laser power (W)	Focal plane position	Surface smoothness Ra(mm)	Height (mm)	Average thickness (mm)	Average Hardness (HV)
1	1.5	200	Small	0.17	5.12	2.4	263
2	1.5	200	Large	0.17	5.26	1.35	262
3	1.5	300	Small	0.13	4.96	2.07	266
4	1.5	300	Large	0.12	6.13	1.73	259
5	2.5	200	Small	0.35	3.69	1.169	259
6	2.5	200	Large	0.3	5.2	2.89	261
7	2.5	200	Small	0.13	3.57	1.86	269
8	2.5	300	Large	0.2	5.36	1.36	262

3.1.Effect of process parameters on the properties of the parts

In this section, the effect of process parameters on the geometry, including the thickness, height, and Hardness of the manufactured parts is investigated.

3.1.1. Effect of process parameters on the thickness and height of the parts

The change in volumetric energy density that is effective on the width of the parts depends on three parameters: laser power, laser focal plane position, and scanning speed. With decreasing energy density, the size of the molten pool decreases, and so, the powder that melts in the molten pool decreases, and as a result, the width of the manufactured parts decreases. As the laser focal plane position increases, due to more interaction area between the laser beam and powder stream, the height of the parts increases. This has also been observed in the research of Nasan et al. [14], who studied the effect of energy density on the height and width of a pass of the DLMD process. In this study, the effect of increasing melt pool temperature on surface stresses of the molten pool, and as a result, the geometry of the molten pool (Fig. 7) is shown.

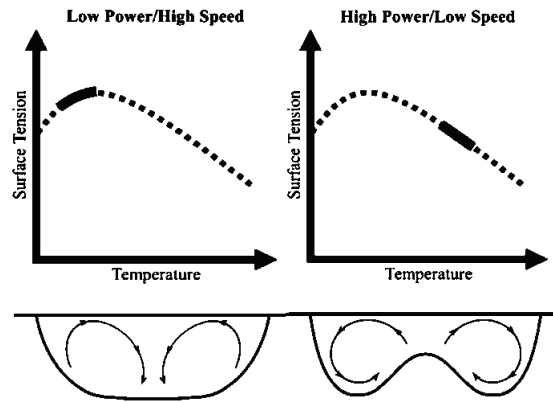


Figure 7 - The effect of increasing the temperature of the molten pool on the geometry of the molten pool [14]. According to Fig. 7, with increasing temperature, surface stresses first increase, and then decrease. As the scanning speed decreases, the temperature of the molten pool increases, and surface stresses cause a change in the direction of rotation of the molten flow in the melt pool. If the direction of rotation is such that it approaches the W-shaped molten pool, the width and height of the parts increase, and the penetration depth of the melt pool in the substrate decreases; and if it rotates oppositely, the width and height of the parts decrease, and the penetration depth of the melt pool increases [14]. According to Equation 3 and Fig. 7, as the laser power increases, the absorbed energy increases and the temperature of the molten pool increases, and as a result, the slope of curves in Fig. 7, which is one of the parameters of the Marangoni relationship, determines the direction of fluid flow in the molten pool. The Marangoni number shows the ratio of surface tension force to viscous force, and also shows the convection flow of liquid metal in the pool. Fig. 8 shows the cross-section of two parts manufactured by high and low power. This figure shows

that the geometry of the molten pool is lower in height and width in low power parts, and the part that is made by higher power has more height and width.

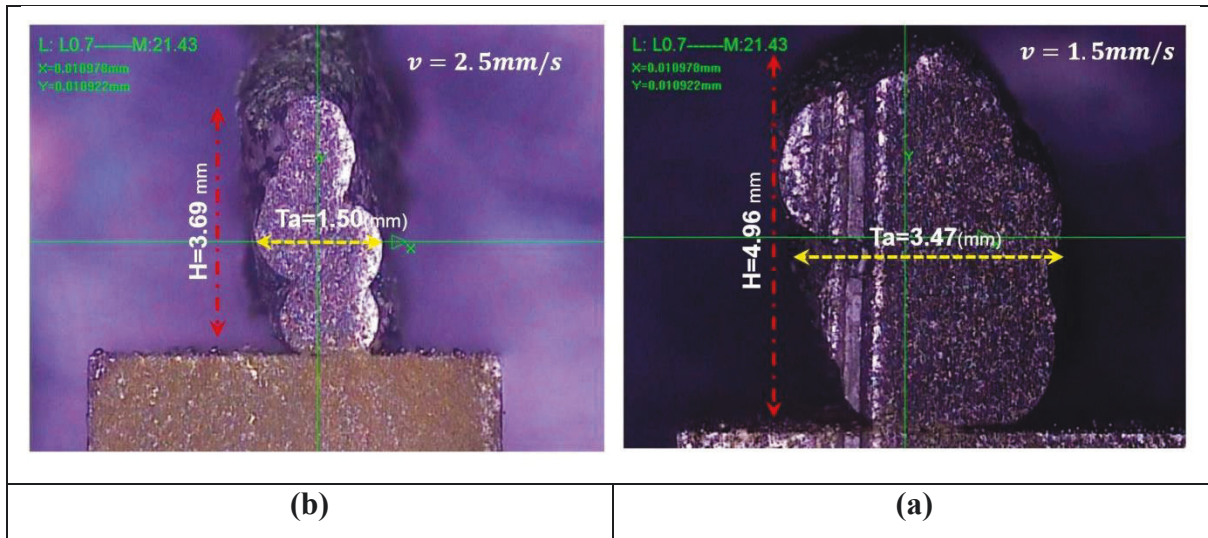


Figure 8- Cross-section of part 3 and 6 a) part 3 with the energy density of 80 W/mm, b) part 6 with the energy density of 200 W/mm.

In addition, the graphs of changes in the height and the thickness of the parts in terms of linear heat input parameter for two positions of the laser lens (2- large diameter and 2+ small diameters) are drawn (Fig. 9 and 10, respectively). The linear energy input is the ratio of the laser power to scanning speed. This value is an index of the absorbed heat in the molten pool that has a significant effect on the geometry of the molten pool, and is calculated from Equation 4.

(4)	$\text{Linear Heat Input} = \frac{\text{Laser Power}}{\text{Table movement Speed}}$
-----	---

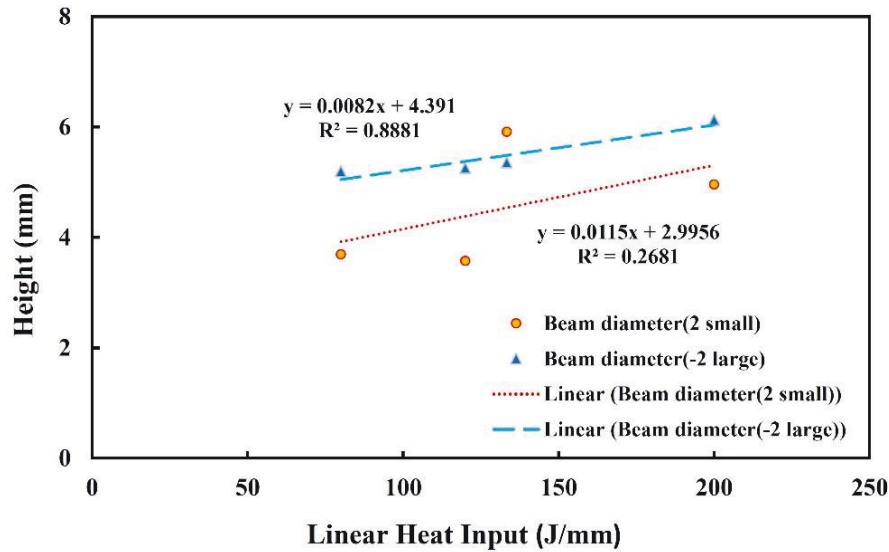


Figure 9- Graph of changes in the height of the parts in terms of linear heat input.

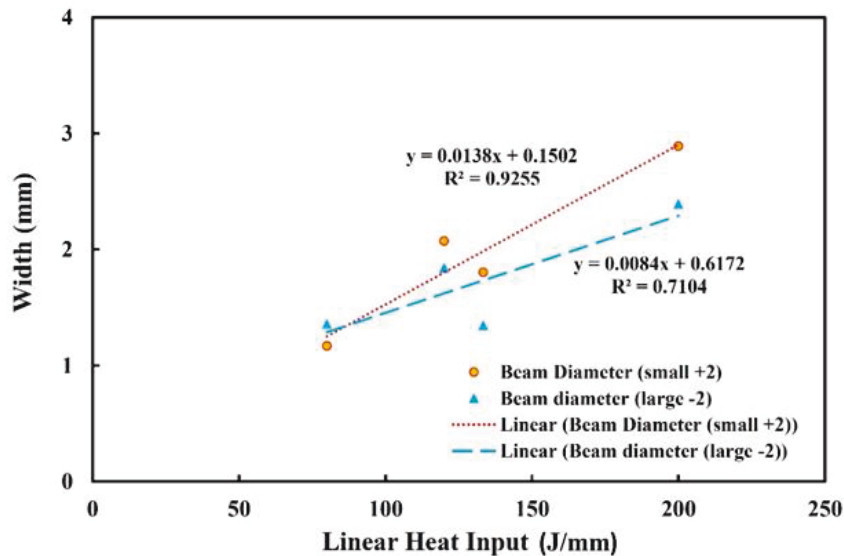


Figure 10- Graph of changes in the width of the parts in terms of linear heat input.

As predicted, the width and height of the parts increase with increasing heat input. The graph in Fig. 9 shows the height of the parts for the case where the laser focal plane position is high. This phenomenon is due to the increase in the effective energy level due to the increase in the laser focal plane position, and this causes more powders to be affected by the laser energy, and increase the absorbed volumetric energy by the molten pool, and as a result, its dimension increase. The graph in Fig. 10 shows that the width of the parts increases with increasing linear heat input. It

also shows the inverse relationship between the laser focal plane position and the thickness of the manufactured parts. This phenomenon occurs due to the Marangoni phenomenon. Fig. 11 shows the cross-sections of two parts manufactured by high and low linear energy densities. As shown in this figure, the thickness and height of the part made with higher linear energy density are more increased.

Increasing the scanning speed reduces the linear heat input. On the other hand, as the scanning speed increases, the powder that sits on the surface decreases. Table 6 shows the effect of increased scanning speed on reducing powder mass used in the process. Following the difference in mass that adheres to the surface, one of the main factors in reducing the height of the parts, manufactured by increasing the laser speed, is the reduction of powder amount that adheres to the surface in each pass. Therefore, it can be said that the scanning speed is one of the most effective parameters on the width and height of the parts.

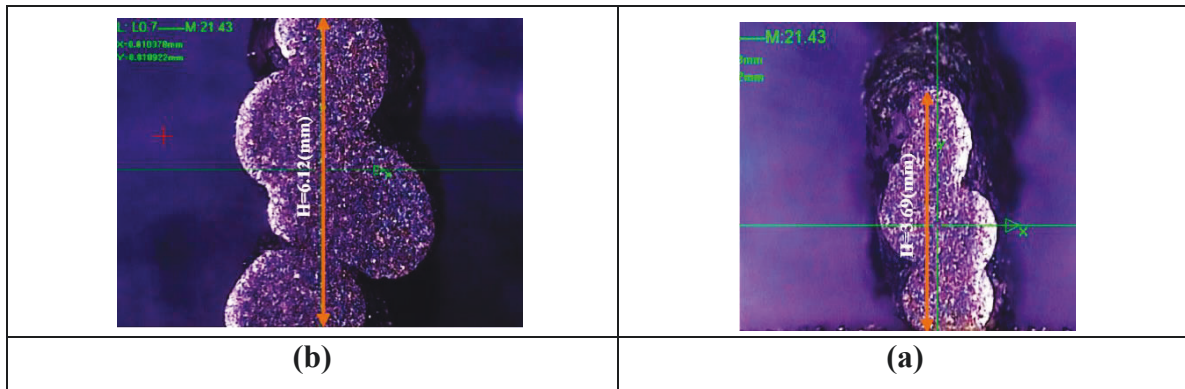


Figure 11 – The height of parts 3 and 7 a) Part 3 with the energy density of 80 w/mm, b) Part 7 with the energy density of 200 w/mm (the variable width can be related to changing the overlapping and scanning speed).

Table 6- mass changes of Powder due to increase in scanning speed

Scanning speed (mm/s)	Time of one pass	Mass of sprayed powder (g)
2.50	8.00	3.40
1.50	13.32	5.66

3.1.2. Effect of process parameters on surface smoothness

Surface smoothness at the ridge of the wall is one of the characteristics of the parts made by AM method. The main factors affecting surface smoothness can be one or more of the factors, including un-melted powder particles, non-fusion of layers, melting range or scanning path strategy, raw materials, including alloy, powder type, particle size distribution (PSD), and powder morphology, design conditions, specific geometry characteristics, flow Melt pool, type of support structure, and process parameters such as laser power, scan speed, layer height, and scanning strategy. If the thickness of the layer increases, the surface smoothness decreases i.e. surface roughness increases [3]. Generally, there are two main causes of surface roughness including the “stair-step effect” and “balling phenomenon”. The ‘stair-step effect’ [15] is due to the stepped approximation by layers of curved and inclined surfaces as shown in Fig. 12 (a). ‘Balling phenomenon’ is due to improper melting of powder particles [16–17]. When a low heat input is used, the energy delivered is insufficient to completely melt the powder particles. The solid powder particles stick at the surfaces of the build (Fig. 12 (b)) [17, 18].

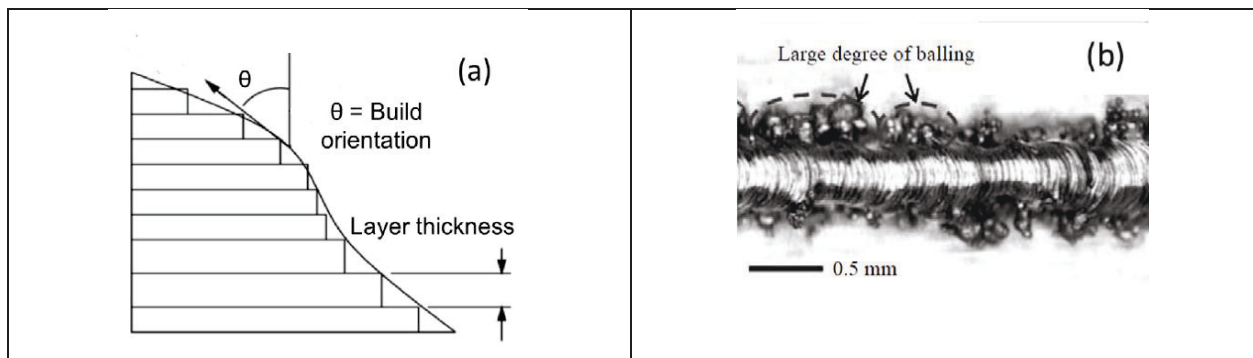


Fig. 12. (a) The stair case effect causing surface roughness [16], (b) balling effect [19]

As the flow rate of the powder sitting on the surface decreases with increasing speed, the thickness of the layers also decreases, which reduces the phenomenon of stepping on the walls of the part. It should be noted that this phenomenon is more pronounced in regions that have a curvature in the direction of layering. The other reason for the formation of rough surfaces is the lack of melting of powder particles and the phenomenon of balling. When the linear input energy is low or the powder is too shiny, the energy absorbed by the powder that causing it to melt is not sufficient. Therefore, solid powder particles stick to structural surfaces. The average surface roughness of un-melted particles is about the diameter of the used powder. At high laser scanning speeds, the molten pool is stretched, destabilizing the molten pool and splitting the surface, which is called islanding.

This process is often described as a balling phenomenon [3]. Due to the flow of molten fluid and the slope of surface tension in the molten pool, these small balls are drawn to the outer edges of the molten pool. Thus, small balls can be found on the lateral edges of the solid path, as shown in Fig. 13.



Figure 13 – Un-melted powders on the surface of the part.

High heat input due to high laser power and low scanning speed melts all the powder particles completely and reduces the balling phenomenon. Therefore, it is expected that the surface roughness will decrease as the heat input increases. The results of earlier studies [3] showed that with increasing linear input energy, regardless of the type of alloy, the surface roughness of AM components decreases. Therefore, the parts manufactured by coarse and glossy powders have a higher surface roughness. Optimization and reduction of surface roughness depend on the interaction of many input parameters and processing conditions. Fig. 14 shows the effect of increasing the linear energy density on the surface roughness. This graph is drawn for two positions (2+ small position and 2-large position) of the lens. The graph shows that, at the same energy density, the surface smoothness for the parts manufactured in the – 2 position is more significant than in the + 2 state. Therefore, the effect of laser focal plane position on surface smoothness is significant, further described in the statistical analysis section. On the other hand, this graph shows that for the small focal plane position, the relationship between linear energy density and surface smoothness is direct. For large focal plane position, no specific trend is observed.

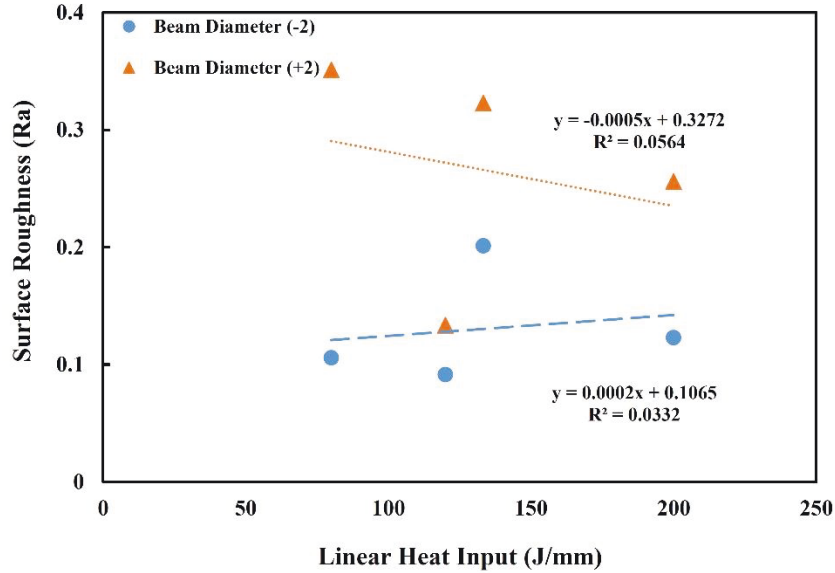


Figure 14- Changes in surface roughness of the parts in terms of linear heat input

The third reason for decreased surface smoothness is the instability of the Kelvin-Helmholtz effect, also known as the Humping phenomenon [3]. Fig. 15 shows the Humping phenomenon in part 4. This phenomenon is caused by the difference between the velocity of the shielding gas and the molten fluid at the surface of the molten pool. In manufactured specimens, this phenomenon is observed at the end of the passes, when the velocity of the shielding gas is higher than the velocity of the molten fluid. Debroy et al. [3] introduced the Richardson number, which is the ratio of gravitational force to surface shear force. They showed that this phenomenon occurs when the Richardson number is less than 0.25.



Figure 15- Humping phenomenon in part 4.

The fourth reason for the decreased surface smoothness is the instability of the rolling plateau. This phenomenon occurs due to the elongation of the molten pool, which is due to the scanning speed, the sharp temperature difference between the molten pool, and the substrate. When the

molten pool is drawn, the passing shape comes out of the cylindrical shape and forms small balls in reducing the scanning speed. Josrow et al. [3] found the optimal dimensions of the molten pool to prevent this phenomenon so that if the ratio of length to width of the molten pool is greater than the π number, this phenomenon occurs. This phenomenon is shown in Fig. 16 for part 2.

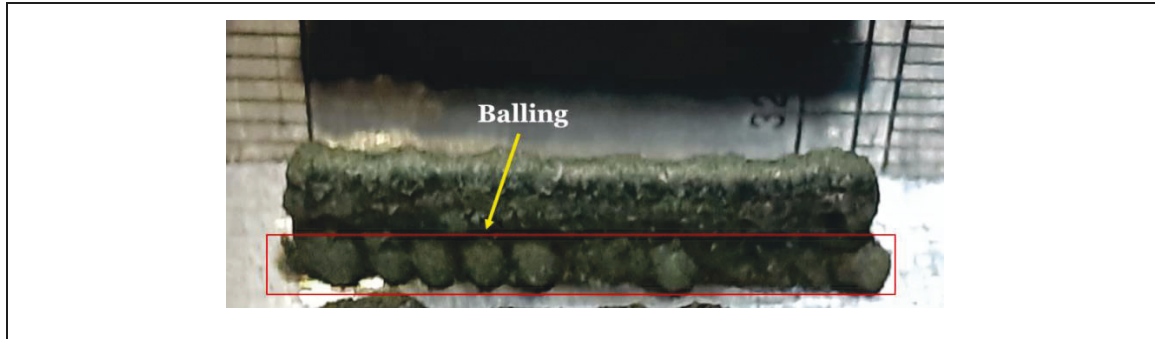


Figure 16- Balling phenomenon in the first layer in the part number (2) with speed (2.5mm/s)

3.1.3. The effect of linear energy density on the penetration depth

The energy transferred from the laser beam to the accumulation area of powder leads to the formation of a molten pool, in addition to the powder collected in that area melts some of the substrates. Therefore, with increasing energy, the penetration depth of the molten pool increases. Fig. 17 shows a schematic of the diffusion of the molten pool in its bottom layer.

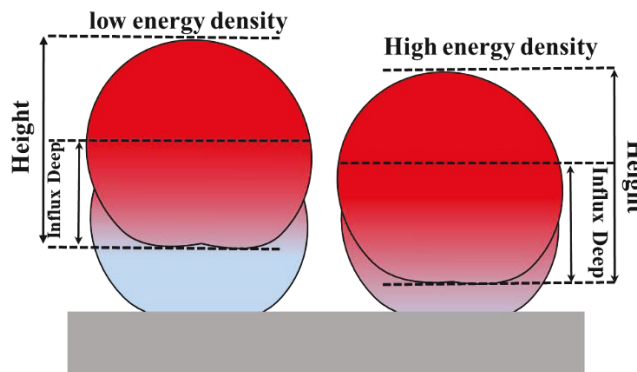


Figure 17. The effect of linear energy density on the penetration depth of manufactured parts.

By layering two passes on top of each other, a valley is created at the border between them. Research by Lin Kwa et al. [12] showed that energy density is directly related to penetration depth and parts with low penetration depth have more porosity than parts with higher penetration depth. According to studies, the optimal penetration depth occurs when the end of the molten pool reaches at least the end of the dendrites of its bottom layer (Fig. 18a). As the linear energy density

increases, the penetration depth of the layers in each other increases. (Fig. 18b) shows the surface profile of two parts with high and low energy density. According to the following figure, it can be seen that increasing the penetration depth increase the smoothness of the surface of the part walls.

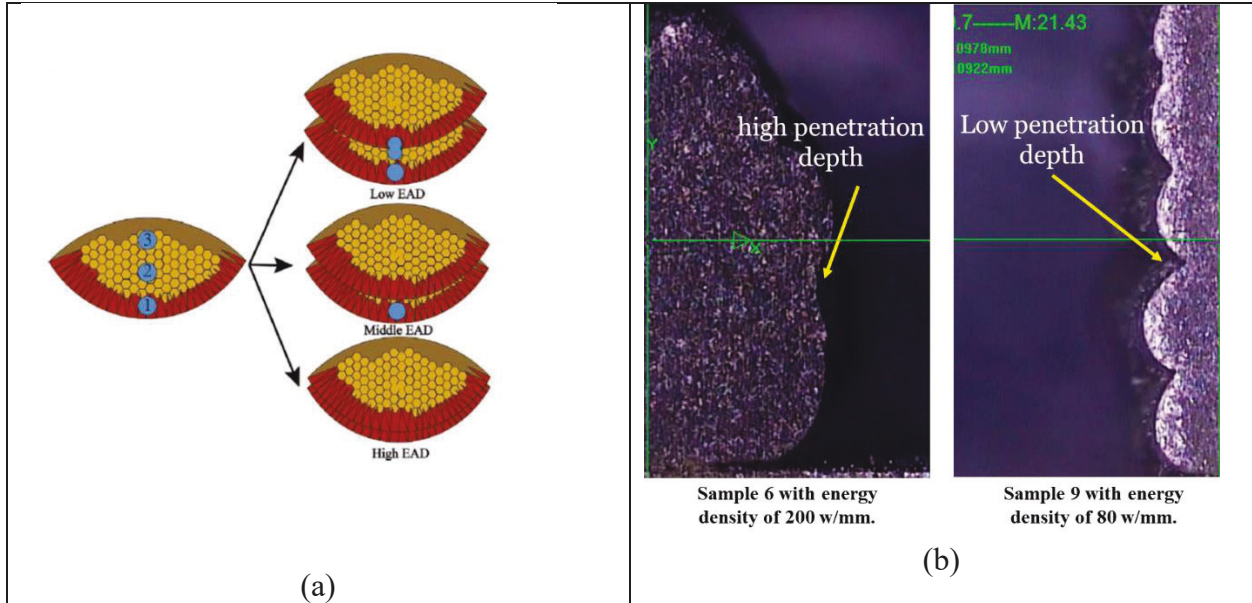


Figure 18 a) Optimal penetration depth of two passes over each other [12] b) Cross-section profiles of two parts with high and low linear energy density.

3.1.4. Effect of process parameters on Hardness

The Hardness variations of the center of the parts made in terms of linear energy density for the two lens positions are plotted in Fig. 19. The chart does not show a specific trend for Hardness, but it can be seen from the graph that when the laser focal plane position increases, the Hardness increases, and with increasing linear input energy, the Hardness decreases. Due to the high heat transfer rate in the DMD process ($10^3 \sim 10^5$ K/s), the Hardness of the parts increases significantly. Most reinforcement elements such as Mo and Nb remain in solid solution in the γ -Ni phase. The Hardness variation of the components is changing in the state of the supersaturated elements in the γ -Ni phase. Inconel 625 alloy is made of solid solution reinforcement and is capable of heat treatment [19].

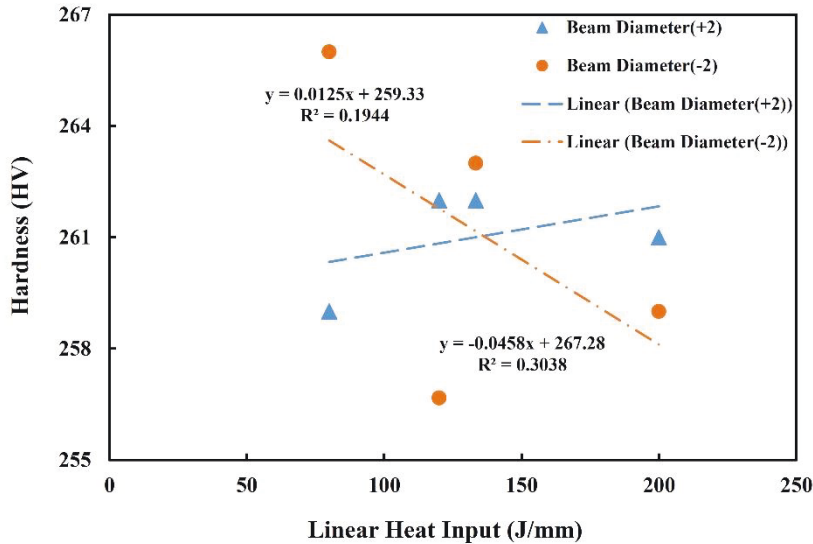


Figure 19- Changes in the stiffness of the center of the parts connecting the energy density

3.2. Statistical analysis

The geometrical dimensions of produced parts (width, height, and surface smoothness), and their Hardness (average surface Hardness) were measured as the output responses of the experiment. Analysis of variance (ANOVA) was applied to investigate significant parameters and their effects. In these analyses, full quadratic polynomial functions were employed using Design-Expert software. The results presented in table 5 can now be analyzed to give information about the width,

height, surface smoothness, and hardness of the parts created, as a function of the changes in process parameters.

3.2.1. The part height

Table 7 shows an analysis of variance for the height of the part. As shown in Table 7, the parameters of scanning speed and laser focal plane position are effective. According to ANOVA of Table 7, equation 5 represents the regression equation for the height of the part considering significant parameters based on coded and actual values, respectively.

$$\text{Height(mm)} = 5.010 - 0.580 \text{ SPEED(mm/s)} - 0.475 \text{ Beam Diameter} \quad (5)$$

Table 7- Revised ANOVA of the height of the part

Source	Degree of freedom	Sum of Squares	Mean Square	F-value	P-value
Model	2	4.496	2.248	7.08	0.035
Linear	2	4.496	2.248	7.08	0.035
SPEED(mm/s)	1	2.687	2.687	8.46	0.033
Beam Diameter	1	1.809	1.809	5.70	0.063
Error	5	1.588	0.317		
Total	7	6.084			
R-Squared= %73.9			R-Squared (Adj)= %63.4		

Fig. 20 depicts the perturbation plot of part height. The perturbation plot can help to compare the effect of all the factors in the central point in the design space. The height of the part is plotted by varying two parameters over its range while the other factor is kept constant. Each line in the plot shows the sensitivity of the part height to the input variables. From the perturbation plot, it is clear that the scanning speed and focal plane position have reverse effects on part height while the laser power has no significant effect on part height. Since the scanning speed and laser focal plane position have a greater slope than the laser power, they have a more significant effect on the part height. According to the graph in Fig. 20, the scanning speed is inversely related to the part height, and the laser focal plane position is directly related to the part height. In addition, the graph shows that by changing the scanning speed and the laser focal plane position, the part height changes by about 1 mm. Therefore, it can be said that the scanning speed and the laser focal plane position are

influential factors in the model. Fig. 21 illustrates the part height response surface based on the input parameters.

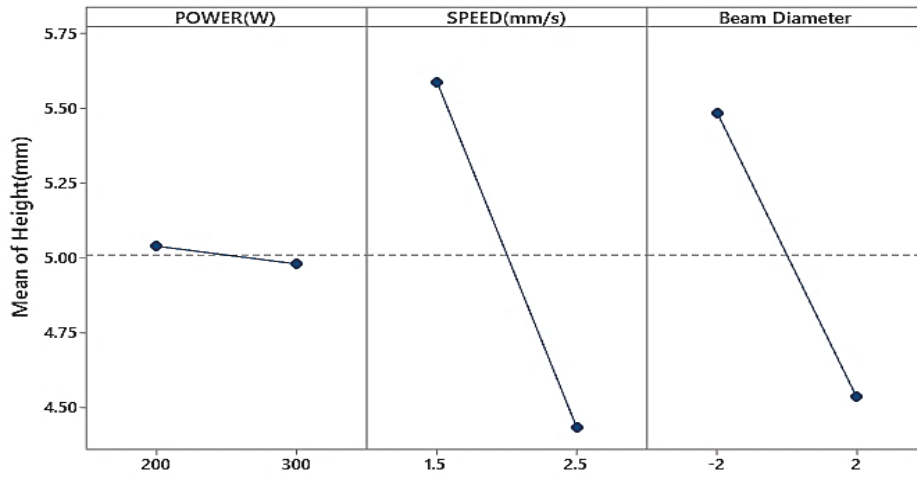


Figure 20- Perturbation plot of part height.

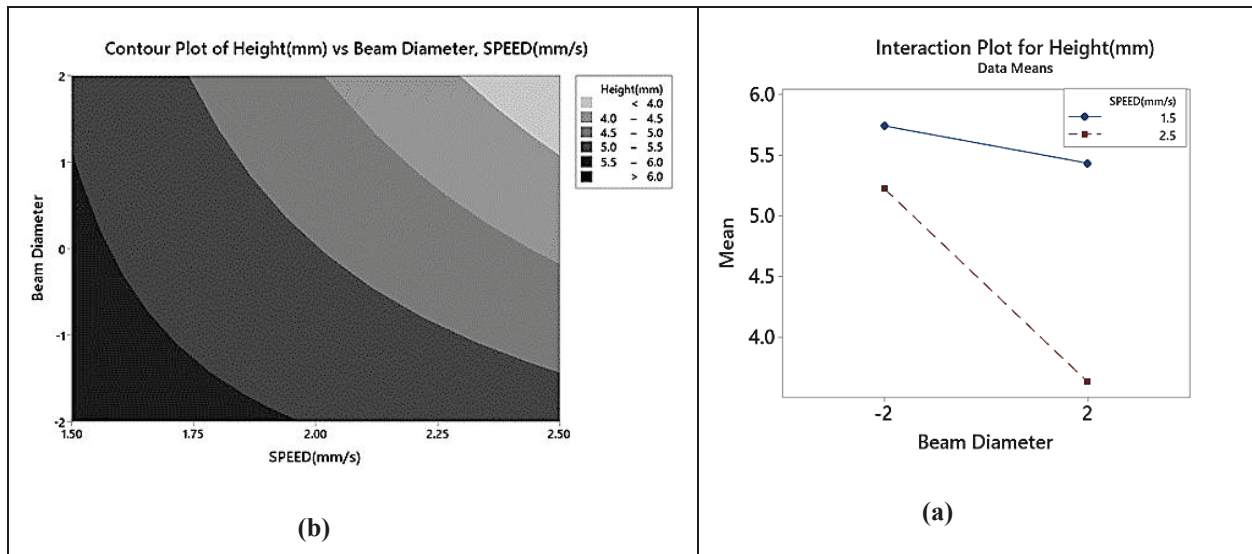


Figure 21- (a) Interactions of laser focal plane position with two scanning speeds of 1.5 mm/s, 2.5 mm/s (b) Height alignment graph in scanning speed and laser focal plane position.

Since the lines do not intersect each other, the interaction of these two parameters cannot affect the model. The alignment graph for height is shown in Figure 19b. The value of the R-sq correlation coefficient is 73.90%. That means that this model is capable of describing 73% of part height changes. In other words, it estimates the part height with 73.90% accuracy.

3.2.2. The part width

The effect of laser speed and power on the width of the parts is much more significant than the laser focal plane position. Since these two parameters affect the linear input energy, and the linear input energy is directly related to the thickness, these two parameters have a more significant effect on the thickness of the molten pool. The regression equation of thickness in terms of scanning speed and laser power is presented in Equation 6. Considering the square value of the correlation coefficient (85.59%), this model can be used to estimate the wall thickness. Variance Analysis, table 8, in the new model shows the P values for laser power and scanning speed (0.005 and 0.044, respectively). This means that the effect of the Marangoni phenomenon has been greater than reducing the powder mass due to the increase in speed.

$$\text{Thickness(mm)} = 1.8590 - 0.4402 \text{ POWER(W)} + 0.2489 \text{ SPEED(mm/s)} \quad (6)$$

Table 8- Variance analysis of thickness for two factors of scanning speed, and laser power

Source	DF	Adj SS	Adj MS	F-Value	P-Value
Model	2	2.0454	1.0227	14.84	0.008
Linear	2	2.0454	1.0227	14.84	0.008
POWER(W)	1	1.5499	1.5499	22.5	0.005
SPEED(mm/s)	1	0.4955	0.4955	7.19	0.044
Error	5	0.3445	0.0689		
Total	7	2.3899			
R-sq = 85.59%			R-sq(adj) = 79.82%		

Fig. 22 shows that the changes in the thickness of the manufactured parts are directly related to the power and laser focal plane position and inversely related to the scanning speed. Since the range of height and slope changes is greater for the power and scanning speed, it seems that the effect of laser power and scanning speed is greater than the laser focal plane position.

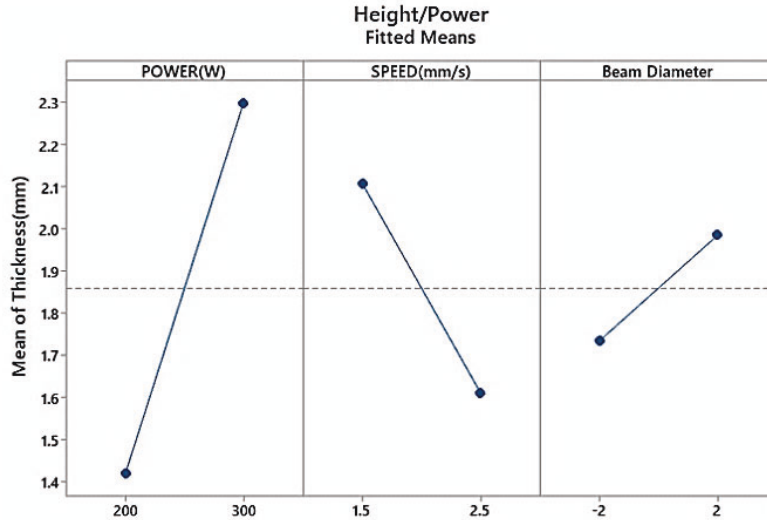


Figure 22 - The effect of the main factors on wall thickness

After examining the interaction of the parameters, it was found that the interaction of the two parameters of laser power and scanning speed has little effect on thickness, which is shown in the interaction graph, Fig. 23. Therefore, since the lines do not intersect each other, their multiplication doesn't affect the response.

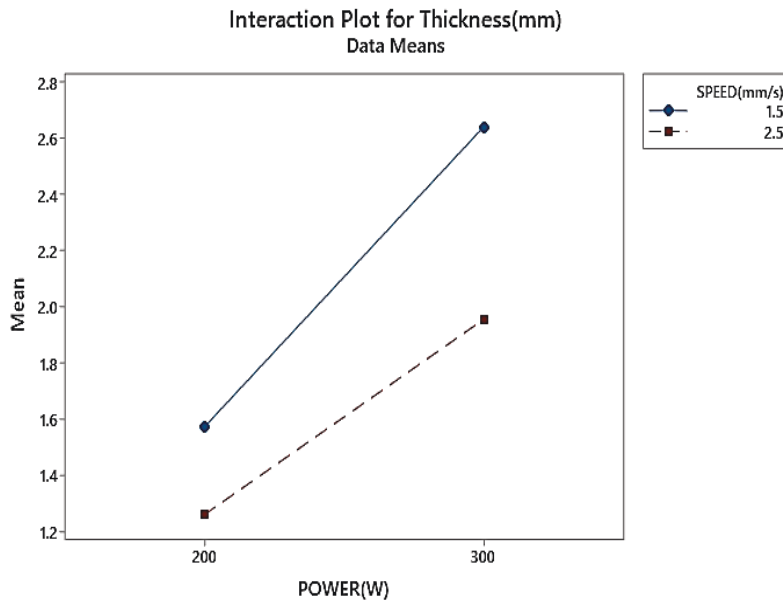


Figure 23 - Interaction effect graph of laser beam diameter with two speeds of 1.5 mm/s, 2.5 mm/s
 In addition, the alignment graph is plotted in Fig. 24 to examine the range of responses.

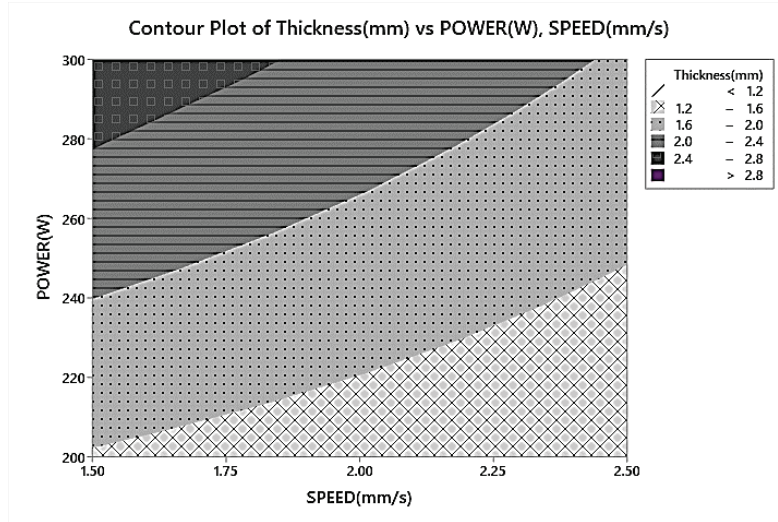


Figure 24 - Thickness alignment graph in terms of scanning speed and laser focal plane position.

3.2.3. The Surface smoothness of part

The table of variance analysis is obtained in Table 9. As can be seen, the P-Value for the power and laser focal plane is less than 0.10. Therefore, it can be said that these factors have a significant effect on surface smoothness.

Table 9- Variance analysis of surface smoothness for two factors of laser power and laser focal plane position.

Source	DF	Adj SS	Adj MS	F-Value	P-Value
Model	2	0.0545	0.0272	7.76	0.029
Linear	2	0.0545	0.0272	7.76	0.029
POWER(W)	1	0.0178	0.0178	5.06	0.074
Beam Diameter	1	0.0367	0.0367	10.46	0.023
Error	5	0.0176	0.0036		
Total	7	0.0720			
R-sq = 75.64%			R-sq(adj) = 65.89%		

Table 9 also shows the values of the R-sq correlation coefficient. According to this coefficient, it can be found that this model can estimate 75.64% of the surface smoothness according to the regression equation presented in Equation. 7.

$$Ra(\text{mm}) = 0.1981 + 0.0471 \text{ POWER(W)} - 0.0677 \text{ Beam Diameter} \quad (7)$$

Fig. 25 shows the main effects of laser power, scanning speed, and laser focal plane on the surface smoothness. This graph shows the power and scanning speed, which is directly related to the surface smoothness and inversely related to the parameter of the laser focal plane position. Since

the laser focal plane position in the -2 mode is larger than in the +2 mode, it can be said that with increasing the focal plane position, the surface smoothness increases. The graph slope of the laser power and the laser focal plane position is greater than the scanning speed, which shows that these two parameters are more effective than scanning speed. This means that in the manufactured parts, the speed is selected in a relatively good range that does not stretch the molten pool.

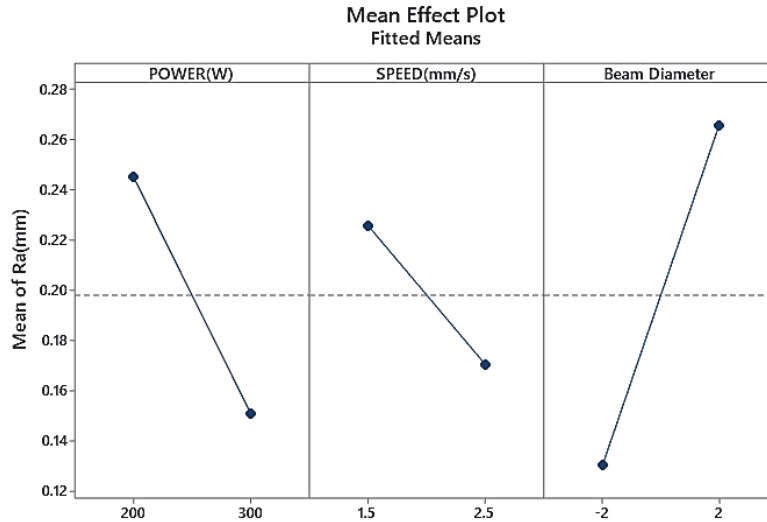


Figure 25- The effect of the main factors on the smoothness of the upper wall surface

To ensure the effectiveness of the laser focal plane, with the same laser power and scanning speed, parts No. 9 and 10 were made, in which the values of the laser focal plane were 4- and +4, respectively. And a sharp difference was observed in the stability of their molten pool. In such a way that, for example, number 10, Due to the severe instability of the molten pool, the molten particles jumped out of the molten pool, and were accompanied by an abnormal sound. While in part number 9, the process was smooth and soundless, and a high-quality part was manufactured. The interaction graph for the two parameters of the focal plane position and laser power is shown in Fig. 26. Since the lines do not intersect each other in this graph, the interaction of the laser power on the laser focal plane has little effect on the surface smoothness. In addition, no specific physical concept for multiplying laser focal plane position by the laser power was observed in the sources.

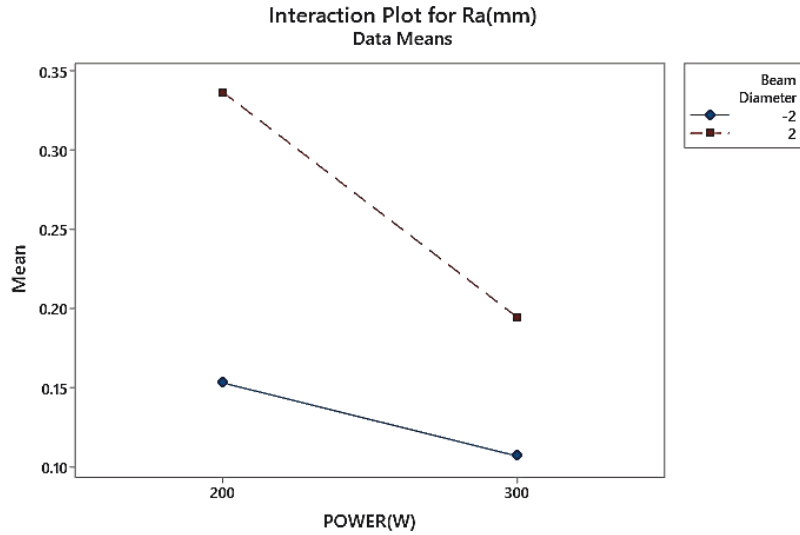


Figure 26- Graph of the interaction of laser power and laser focal plane with two levels (2- and +2). Fig. 27 shows the alignment graph to estimate the surface smoothness of the parts manufactured by two significant factors of laser power and laser focal plane position. Therefore, the graphs of Fig. 26 can be used to estimate the surface smoothness range.

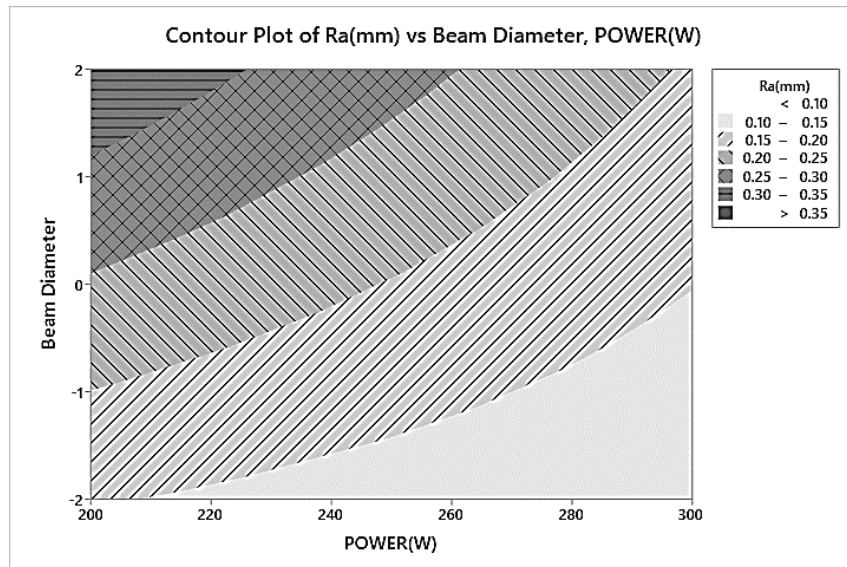


Figure 27- Alignment Graph of surface smoothness, in terms of scanning speed and laser focal plane position.

3.2.4. Average Hardness of the part

Table of variance Analysis, Table 10, shows that the considered parameters do not have a significant effect on the average Hardness of the parts, and the part Hardness does not follow a

specific trend. However, the effect of laser power on Hardness is more significant than other parameters, and this is due to changes in the temperature of the molten pool and the cooling time of the parts.

Table 10 - variance analysis of average Hardness

Source	DF	Adj SS	Adj MS	F-Value	P-Value
Model	3	16.323	5.441	0.53	0.688
Linear	3	16.323	5.441	0.53	0.688
POWER(W)	1	16.046	16.046	1.55	0.281
SPEED(mm/s)	1	0.221	0.221	0.02	0.891
Beam Diameter	1	0.056	0.056	0.01	0.945
Error	4	41.369	10.342		
Total	7	57.693			

4. Conclusion

In this research, the process parameters of direct laser metal deposition, including laser power, scanning speed, and laser focal plane on the geometry and quality of the components were examined. The results showed that:

- By increasing the scanning speed, the height and width of the manufactured parts decreases, and increasing the scanning speed too much causes the molten pool to stretch, and the balling phenomenon to form. On the other hand, reducing the scanning speed increases the energy density and instability of the molten pool, and creates porosity due to the evaporation of some materials in the powder.
- As the scanning speed increases, the surface smoothness decreases.
- Increasing laser focal plane position reduces the height and width of the parts due to the decrease in the density of volumetric energy absorbed by the molten pool.
- According to statistical analysis, the effect of laser power on the width of the manufactured parts has a more significant effect than the scanning speed due to the Marangoni phenomenon.
- Input linear heat is directly related to the surface smoothness.

References

A. Beiker Kair and K. Sofos, "Additive manufacturing and production of metallic parts in automotive industry: A case study on technical, economic, and environmental sustainability aspects," ed, 2014.	[1]
F. Wirth, S. Arpagaus, and K. Wegener, "Analysis of melt pool dynamics in laser cladding and direct metal deposition by automated high-speed camera image evaluation," <i>Additive Manufacturing</i> , vol. 21, pp. 369-382, 2018.	[2]
T. DebRoy et al., "Additive manufacturing of metallic components—process, structure, and properties," <i>Progress in Materials Science</i> , vol. 92, pp. 112-224, 2018.	[3]
R. Koike et al., "Evaluation for mechanical characteristics of Inconel625–SUS316L joint produced with direct energy deposition," <i>Procedia Manufacturing</i> , vol. 14, pp. 105-110, 2017.	[4]
I. Taberero, A. Lamikiz, S. Martínez, E. Ukar, and J. Figueras, "Evaluation of the mechanical properties of Inconel 718 components built by laser cladding," <i>International Journal of Machine Tools and Manufacture</i> , vol. 51, no. 6, pp. 465-470, 2011.	[5]
R. Ghanavati, H. Naffakh-Moosavy, M. Moradi " Additive Manufacturing of Thin-Walled SS316L-IN718 Functionally Graded Materials by Direct Laser Metal Deposition," <i>Journal of Materials Research and Technology</i> , vol. 15, pp. 2673-2685, 2021.	[6]
P. Ganesh et al., "Fatigue and fracture toughness characteristics of laser rapid manufactured Inconel 625 structures," <i>Materials Science and Engineering: A</i> , vol. 527, no. 29-30, pp. 7490-7497, 2010.	[7]
J. Mazumder, D. Dutta, N. Kikuchi, and A. Ghosh, "Closed-loop direct metal deposition: art to part," <i>Optics and Lasers in Engineering</i> , vol. 34, no. 4-6, pp. 397-414, 2000.	[8]
M. Moradi, A. Hasani, Z. Malekshahi Beiranvand, A. Ashoori, "Additive manufacturing of stellite 6 superalloy by direct laser metal deposition – Part 2: Effects of scanning pattern and laser power reduction in different layers", <i>Optics & Laser Technology</i> , Volume 131, 2020, 106455.	[9]
M. Moradi, A. Hasani, A. Ashoori, "Additive manufacturing of stellite 6 superalloy by direct laser metal deposition – Part 1: Effects of laser power and focal plane position", <i>Optics & Laser Technology</i> , Volume 131, 2020, 106328.	[10]
M. Moradi, A. Hasani, Z. Pourmand, J. Lawrence., "Direct laser metal deposition additive manufacturing of Inconel 718 superalloy: Statistical modelling and optimization by design of experiments", <i>Optics and Laser Technology</i> , Volume 144, 2021, (107380)	[11]
L. Cao et al., "Effect of laser energy density on defects behavior of direct laser depositing 24CrNiMo alloy steel," <i>Optics & Laser Technology</i> , vol. 111, pp. 541-553, 2019.	[12]
S. H. Oliari, A. S. C. M. D'Oliveira, and M. Schulz, "Additive manufacturing of H11 with wire-based laser metal deposition," <i>Soldagem & Inspeção</i> , vol. 22, no. 4, pp. 466-479, 2017.	[13]
N. A. Kistler, A. R. Nassar, E. W. Reutzel, D. J. Corbin, and A. M. Beese, "Effect of directed energy deposition processing parameters on laser deposited Inconel 718: Microstructure, fusion zone morphology, and Hardness," <i>Journal of Laser Applications</i> , vol. 29, no. 2, p. 022005, 2017.	[14]

E. A. Lass et al., "Formation of the Ni ₃ Nb δ -phase in stress-relieved Inconel 625 produced via laser powder-bed fusion additive manufacturing," <i>Metallurgical and Materials Transactions A</i> , vol. 48, no. 11, pp. 5547-5558, 2017.	[15]
Rahmati S, Vahabli E. Evaluation of analytical modeling for improvement of surface roughness of FDM test part using measurement results. <i>Int J Adv Manuf Technol</i> 2015;79(5-8):823-9	[16]
Kruth JP, Froyen L, Van Vaerenbergh J, Mercelis P, Rombouts M, Lauwers B. Selective laser melting of iron-based powder. <i>J Mater Process Technol</i> 2004;149(1-3):616-22.	[17]
Gu DD, Shen YF. Balling phenomena in direct laser sintering of stainless steel powder: metallurgical mechanisms and control methods. <i>Mater Des</i> 2009;30(8):2903-10.	[18]
Mumtaz K, Hopkinson N. Top surface and side roughness of Inconel 625 parts processed using selective laser melting. <i>Rapid Prototyp J</i> 2009;15 (2):96-103.	[19]